Soares, G. B., Yamazaki, Y., Matzka, J., Pinheiro, K., Morschhauser, A., Stolle, C., Alken, P. (2018): Equatorial Counter Electrojet Longitudinal and Seasonal Variability in the American Sector. - *Journal of Geophysical Research*, *123*, 11, pp. 9906—9920.

DOI: http://doi.org/10.1029/2018JA025968

Journal of Geophysical Research: Space Physics

RESEARCH ARTICLE
10.1029/2018JA025968

Equatorial Counter Electrojet Longitudinal and Seasonal Variability in the American Sector

Gabriel Soares[1], Yosuke Yamazaki[2], Jürgen Matzka[2], Katia Pinheiro[1], Achim Morschhauser[2], Claudia Stolle[2,3], and Patrick Alken[4,5]

[1]Observatório Nacional, Rio de Janeiro, Brazil, [2]GFZ German Research Centre for Geosciences, Potsdam, Germany, [3]Faculty of Science, University of Potsdam, Potsdam, Germany, [4]Cooperative Institute for Research in Environmental Sciences, University of Colorado Boulder, Boulder, CO, USA, [5]National Centers for Environmental Information, NOAA, Boulder, CO, USA

Key Points:
- A 10-year ground-based data set was used to investigate counter electrojet climatology in the Brazilian sector for the first time
- A comparison with the Peruvian sector counter electrojet climatology reveals a longitudinal variability around the June solstice
- Besides the known wave-4 structure, migrating tides play a role for the counter electrojet longitudinal dependence in South America

Correspondence to:
G. Soares,
gabrielsoares@on.br

Citation:
Soares, G., Yamazaki, Y., Matzka, J., Pinheiro, K., Morschhauser, A., Stolle, C., & Alken, P. (2018). Equatorial counter electrojet longitudinal and seasonal variability in the American sector. *Journal of Geophysical Research: Space Physics*, *123*, 9906–9920. https://doi.org/10.1029/2018JA025968

Received 2 AUG 2018
Accepted 30 OCT 2018
Accepted article online 9 NOV 2018
Published online 28 NOV 2018

Abstract The equatorial electrojet occasionally reverses during morning and afternoon hours, leading to periods of westward current in the ionospheric E region that are known as counter electrojet (CEJ) events. We present the first analysis of CEJ climatology and CEJ dependence on solar flux and lunar phase for the Brazilian sector, based on an extensive ground-based data set for the years 2008 to 2017 from the geomagnetic observatory Tatuoca (1.2°S, 48.5°W), and we compare it to the results found for Huancayo (12.0°S, 75.3°W) observatory in the Peruvian sector. We found a predominance of morning CEJ events for both sectors. The afternoon CEJ occurrence rate in the Brazilian sector is twice as high as in the Peruvian sector. The afternoon CEJ occurrence rate strongly depends on season, with maximum rates occurring during the northern-hemisphere summer for the Brazilian sector and during the northern-hemisphere winter for the Peruvian sector. Significant discrepancies between the two sectors are also found for morning CEJ rates during the northern-hemisphere summer. These longitudinal differences are in agreement with a CEJ climatology derived from contemporary Swarm satellite data and can be attributed in part to the well-known longitudinal wave-4 structure in the background equatorial electrojet strength that results from nonmigrating solar tides and stationary planetary waves. Simulations with the Thermosphere-Ionosphere-Electrodynamics General Circulation Model show that the remaining longitudinal variability in CEJ during northern summer can be explained by the effect of migrating tides in the presence of the varying geomagnetic field in the South Atlantic Anomaly.

1. Introduction

Records from ground magnetometers at the magnetic equator show a large daily variation in the horizontal component H of the geomagnetic field, reaching amplitudes of a few hundred nanotesla (Chapman & Bartels, 1940). The solar quiet (Sq) daily variation within a narrow band of about 4° from the magnetic equator is characterized by an additional signal caused by the equatorial electrojet (EEJ; Chapman, 1951). The EEJ is a zonal electric current directed eastward that flows at a height of about 105 km in the ionosphere E region (Pfaff et al., 1997). The peak current density of the EEJ is typically 5–10 $\mu A/m^2$, which is one order of magnitude stronger than the Sq currents at middle and low latitudes. The EEJ causes a horizontal magnetic field directed approximately northward at ground stations below it, leading to an enhancement of the measured H-component daily variation. For a comprehensive review on the EEJ, we refer to Yamazaki and Maute (2017).

The occurrence of depressions in H during daytime at the magnetic equator is a well-known phenomenon (e.g., Denardini et al., 2009; Doumouya et al., 1998; Gouin & Mayaud, 1967; Gurubaran, 2002; Marriott et al., 1979; Mayaud, 1977; Onwumechili & Akasofu, 1972; Patil et al., 1990a, 1990b; Rabiu et al., 2017; Rastogi, 1974a; Rastogi et al., 2014; Venkatesh et al., 2015). These depressions are caused by westward currents in the equatorial ionospheric E region, that is, currents flowing opposite to the normal eastward EEJ. They are referred to as counter electrojet (CEJ) events, which can occur during both geomagnetically quiet and disturbed periods, differing in their triggering mechanisms.

The quiet-time CEJ is mainly related to changes in the atmospheric tides that dominate the global wind system at ionospheric heights (Gurubaran, 2002; Hanuise et al., 1983), and it is mostly observed during a few hours in the morning (MCEJ) or afternoon (ACEJ) periods. Under disturbed conditions, other mechanisms play a role in addition to the tidal variability, such as the prompt penetration of polar electric field into equatorial

latitudes and the disturbance dynamo electric field (Kikuchi et al., 2003, 2008; Rastogi, 1977; Yamazaki & Kosch, 2015; Zhang, Liu, Le, & Chen, 2017).

Rastogi (1974a) and Marriott et al. (1979) showed that the occurrence of ACEJ events is clearly anticorrelated with the sunspot number, whereas a less obvious relation is typically observed for MCEJ. Fang et al. (2014), using a numerical model, showed how lower solar activity conditions are favored for the occurrence of ACEJ. They discussed that lower solar flux levels lead to a decrease in the atmosphere ionization rates and to lower ionospheric conductivities, causing less intense EEJ current and favoring downward plasma drifts in the ionosphere during the afternoon (i.e., ACEJ occasions). On the other hand, Gouin and Mayaud (1967) and Patil et al. (1990b) indicated that higher MCEJ rates may be related to solar maximum periods.

Lunar gravitational tides are also known to modulate the occurrence of CEJ. Studies have shown that the occurrence rate of CEJ is clearly dependent on the lunar phase (Fejer et al., 2010; Marriott et al., 1979; Onwumechili & Akasofu, 1972; Patil et al., 1990a, 1990b; Rastogi, 1974b). Occasionally, sudden stratospheric warming events occur during the northern hemisphere winter, affecting the lunar tides and increasing CEJ rates (Fejer et al., 2010; Stening et al., 1996; Yamazaki, 2013).

It is well established that nonmigrating tides and stationary planetary waves play an important role in the longitudinal variation of the daytime EEJ intensity. In particular, the eastward-propagating nonmigrating tide with zonal wavenumber 3 (DE3) has been identified as the primary cause of the so-called wave-4 longitudinal structure in the ionosphere (Lühr & Manoj, 2013; Lühr et al., 2008). The DE3 is mainly generated by solar radiation and latent heat release in the tropical troposphere. The tidal wave propagates vertically upward from its source region and transfers energy and momentum into the E-region ionosphere before being dissipated (Hagan & Forbes, 2002; Hagan et al., 2007; Oberheide et al., 2009). At a fixed local time, the effect of DE3 on the ionosphere appears as a longitudinal structure with four peaks (e.g., Immel et al., 2006). This wave-4 structure has been observed in the E-region electric fields and in the EEJ (England et al., 2006; Kil et al., 2007; Lühr et al., 2008).

Recently, Singh et al. (2018) used magnetometer data from the Challenging Minisatellite Payload satellite and zonal wind observations from the Thermosphere Ionosphere Mesosphere Energetics and Dynamics satellite to demonstrate that the occurrence rate of ACEJ on a global scale is strongly influenced by the DE3 tidal mode during July–September months. They observed longitudinal sectors of high ACEJ occurrence that coincide with regions of eastward DE3 tidal winds. Their study was limited to the afternoon hours, and the relationship between the DE3 eastward wind and ACEJ did not hold in some longitude sectors (especially in the West Pacific sector), indicating that there are additional sources of CEJ longitudinal variability. Archana et al. (2018) also related the CEJ longitudinal variability to the DE3 tide, using geomagnetic ground data from three closely spaced stations in the Indian sector.

Pandey et al. (2018) studied the cause of higher occurrence rates of ACEJ during the northern summer months over the Indian sector, by using the EEJ model from Anandarao (1976) and the empirical vertical drift model from Fejer et al. (2008). They showed that the ACEJ can result from westward quiet-time electric fields (manifested as downward drifts in Fejer et al., 2008, model) and suggested a global nature for such events (see also Gurubaran, 2002).

In this study, we want to investigate the CEJ occurrence rate during geomagnetically quiet periods in the Brazilian and Peruvian sectors and explain the longitudinal differences in the CEJ rates within South America. To this end, we analyze ground-based and satellite-based magnetometer data as well as simulations from the Thermosphere-Ionosphere-Electrodynamics General Circulation Model (TIEGCM).

2. Data and Model

2.1. Ground-Based Magnetometer Data

The magnetic signal of the EEJ/CEJ is localized near the magnetic equator, and it can be isolated from the large-scale magnetic fields due to the global Sq current system and magnetospheric currents by taking the difference (ΔH) of the geomagnetic field H component measured at an equatorial station and a low-latitude station at a similar longitude but outside the influence of the EEJ (e.g., such as in Stolle et al., 2008). To apply this technique, we used 1-min ground magnetometer data to detect MCEJ and ACEJ occurrences in the American sector from June 2008 to December 2017.

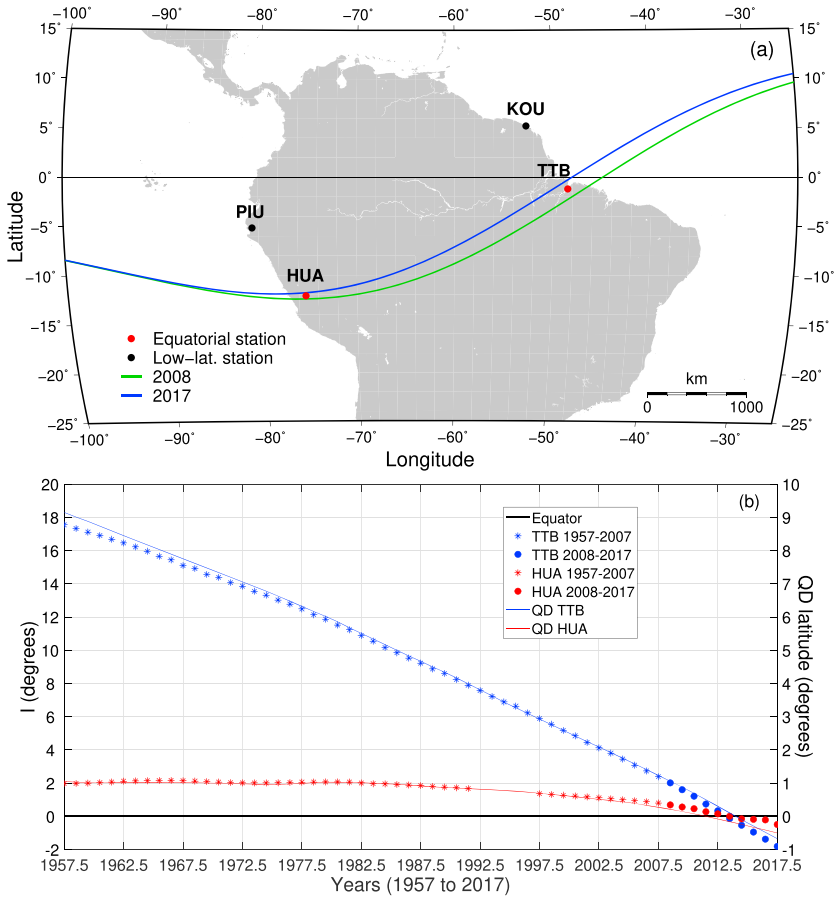

Figure 1. (a) Map (equidistant Hammer projection) of ground magnetometers at TTB and KOU (850-km distance, Brazilian sector) and, 26.8° in longitude further westward, at HUA and PIU (960-km distance, Peruvian sector). The magnetic equator is indicated for 2008 (green) and 2017 (blue). (b) Annual means of geomagnetic inclination I (asterisk prior to 2008 and circles for the period studied here from 2008 to 2017) and QD latitude for TTB (blue line) and HUA (red line) from 1957 to 2017. The horizontal thick black line indicates $I = 0°$ (magnetic equator). TTB = Tatuoca; KOU = Kourou; HUA = Huancayo; PIU = Piura; QD = quasi-dipole.

For the Brazilian sector, data from the geomagnetic observatories Tatuoca (TTB, 1.2°S, 48.5°W) and Kourou (KOU, 5.2°N, 52.7°W) were used as equatorial and low-latitude data, respectively. For TTB, we calibrated a data set from existing fluxgate raw data from 2008 to 2017, which is available as a data publication (Soares et al., 2018) at GFZ Data Services (http://dataservices.gfz-potsdam.de/portal/). For KOU, definitive (prior to 2014) and quasi-definitive (2014 onward) INTERMAGNET data were used (www.intermagnet.org). The equatorial geomagnetic observatory Huancayo (HUA, 12.0°S, 75.3°W) and the low-latitude magnetometer station Piura (PIU, 5.2°S, 80.6°W) were used for the Peruvian sector. HUA data were taken from INTERMAGNET (definitive data for 2008 to 2015 and preliminary data for 2016 and 2017). PIU data were downloaded from the LISN network (Valladares & Chau, 2012) website (http://lisn.igp.gob.pe/data/). The percentage of available H-component data for each station is 89% (TTB), 99% (KOU), 98% (HUA), and 83% (PIU), resulting in a data availability of 88% and 82% for the pairs TTB-KOU and HUA-PIU, respectively. For information on TTB, Morschhauser et al. (2017) is referred. More details on geomagnetic observatories and INTERMAGNET can be found in Matzka et al. (2010) and Chulliat et al. (2016).

Figure 1a shows the location of the stations from the Brazilian and Peruvian sectors. The geographic equator and the positions of the magnetic equator (predicted by the International Geomagnetic Reference Field model (IGRF-12); Thébault et al., 2015) for 2008 and 2017 are also indicated. TTB is very close to both the geographic and the magnetic equator. This is also the region with the strongest secular variation of the geomagnetic inclination I with around −0.4°/year (variations in I ranges from −0.4° to +0.1°/year, according to

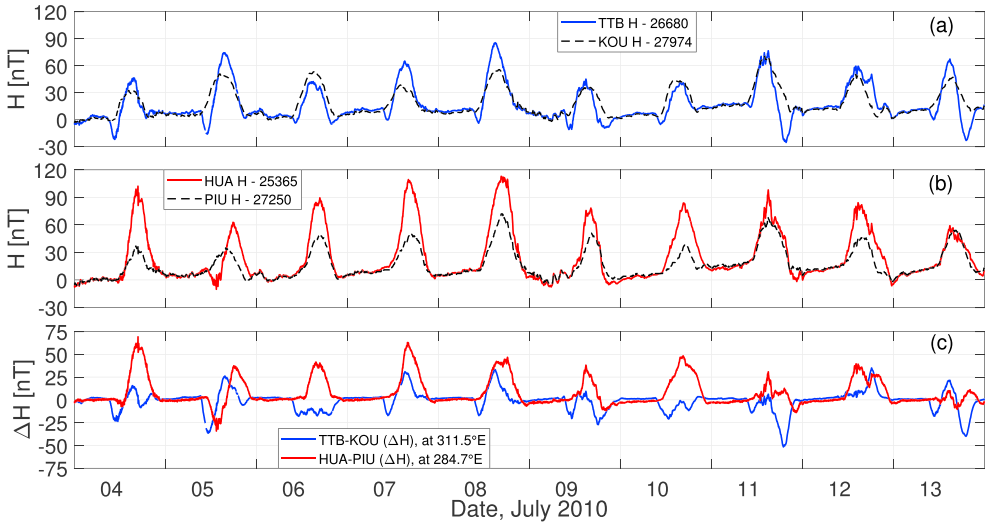

Figure 2. H-component of the geomagnetic field (nighttime values subtracted) at TTB (a, in blue) and HUA (b, in red) for 10 days in July 2010. Corresponding low-latitude stations (KOU and PIU) H values are shown as black-dashed lines. (c) ΔH representing the equatorial electrojet signals for the Brazilian (TTB-KOU, blue) and Peruvian (HUA-PIU, red) sectors. Time is in UT. TTB = Tatuoca; KOU = Kourou; HUA = Huancayo; PIU = Piura.

IGRF-12). This is shown in Figure 1b by annual means of I at TTB (since its installation in 1957), including comparison with the nearly constant I values for HUA and their quasi-dipole latitude values (Emmert et al., 2010). The rapid change of I in the Brazilian sector corresponds to a northward movement of the magnetic equator by about 22 km/year, which can be seen in Figure 1a as the displacement of the magnetic equator position from 2008 to 2017. It is worth mentioning that, at the location of TTB, the angle between the geographic equator and the magnetic equator is the largest. On the other hand, HUA is located at the southernmost point of the magnetic equator, where it is nearly parallel to the geographic equator.

During the period of data used in this study, the quasi-dipole latitude of TTB varied from 1.1° to −0.7°, while at HUA, it changed from 0.2° to −0.5° (Figure 1b, blue and red lines). At KOU and PIU, the magnetic latitude changed from 9.1° to 7.4° and from 6.7° to 6.2°, respectively. The ΔH calculated from an equatorial station within +/−3° of the magnetic equator and a low-latitude station at a distance of around 6° to 9° from the magnetic equator is an ideal measure for the EEJ (Anderson et al., 2006; Yamazaki & Maute, 2017; Yizengaw et al., 2014). The stations used in this work fit these intervals.

An example of H-component variation (with nighttime values subtracted) for the Brazilian (TTB and KOU) and Peruvian (HUA and PIU) sectors is shown in Figures 2a and 2b for 10 consecutive days in July 2010. Section 4 describes in more detail the determination of precise nighttime values. Note the enhanced noontime values at TTB and HUA when compared to KOU and PIU in Figures 2a and 2b. Figure 2c shows ΔH for the pairs TTB-KOU and HUA-PIU, where a clear day-to-day and longitudinal variability in the EEJ is seen. For the period considered in Figure 2c, the EEJ is weaker, and the CEJ events (depressions in ΔH) are more frequent and intense in the Brazilian sector than in the Peruvian sector.

Rastogi (1974a), Marriott et al. (1979), and more recently Rabiu et al. (2017) compared the CEJ climatology at several longitudes, but HUA was the only source of data from South America. Other previous studies have compared the EEJ characteristics at the Peruvian and Brazilian sectors, but data from the latter sector were often limited in time (Kane & Trivedi, 1981; Rastogi & Yumoto, 2006; Rastogi, Chandra, Rahul, et al., 2013). Kane and Trivedi (1982), Shume et al. (2010), and Yizengaw et al. (2014) noted differences in the seasonal variations of the EEJ in the Brazilian and Peruvian sectors using, 1, 2, and 4 years of data, respectively. All found a higher average EEJ intensity in the Peruvian sector (as seen for the period depicted in Figure 2). Kane and Trivedi (1981) found higher CEJ rates in the Brazilian sector than in the Peruvian sector, but their analysis is restricted to six magnetically quiet days during September 1970, only. Denardini et al. (2009) examined selected CEJ events observed in the Brazilian sector. They compared the data from ground-based magnetometer, RESCO radar, and digital sounder. Vichare and Rajaram (2011), using 60 days of Ørsted satellite

observations, found the highest CEJ rates worldwide in the Brazilian sector. Venkatesh et al. (2015) analyzed the EEJ variability and its effect on the equatorial ionization anomaly (EIA) in the Brazilian sector, as well as in the Indian sector. They showed that the EIA is not fully formed when there is a well-developed MCEJ. Stolle et al. (2008) analyzed the development of the EIA related to CEJ occurrence at any local time at the HUA sector. They found that the EIA reduces after CEJ onsets and develops after the CEJ ceased with a response time of about 4 hr. Compared to previous studies, TTB provides a comprehensive 10-year data set to study CEJ climatology in the Brazilian sector.

2.2. Swarm Satellite Data

The Swarm mission was launched in November 2013 by the European Space Agency to investigate the geomagnetic field. It is a constellation of three identical satellites with circular orbits with periods of around 1.5 hr. Two satellites (Swarm A and C) fly side-by-side at 460-km (initial) height with an inclination of 87.4°. The third spacecraft (Swarm B) flies at a higher (initial) orbit of 530-km height and with 88° of inclination (Friis-Christensen et al., 2006, 2008). In this work we use magnetic field measurements from Swarm A and B during November 2013–May 2017. The EEJ current intensity was derived from the magnetometer data using the method described in Alken et al. (2013, 2015). First, model predictions of the magnetic fields of non-ionospheric origin (i.e., the core, lithospheric, and magnetospheric fields) are subtracted from the original data. Then, the residual fields are separated into the large-scale Sq (and residual magnetospheric) field and the EEJ field that is localized near the magnetic equator. Finally, the EEJ field is inverted for the EEJ current, based on a line-current model and the Biot-Savart law.

2.3. Geophysical Indices

The Kp index provided by GFZ German Research Centre for Geosciences (ftp://ftp.gfzpotsdam.de/pub/home/obs/kp-ap/) was used as criterion for magnetically quiet periods. The monthly averages of the observed F10.7 index for solar radio flux data were taken from Natural Resources Canada (http://www.spaceweather.ca/solar-flux/sx-en.php) and used to investigate the solar flux effects on the CEJ phenomenon.

2.4. TIEGCM

The TIEGCM is a first-principles model of the coupled thermosphere-ionosphere system developed at the National Center for Atmospheric Research (Qian et al., 2014; Richmond et al., 1992). The model solves the continuity, momentum, and energy equations for the altitude range of approximately 97–600 km with a horizontal grid resolution of 5° times 5°. Electric fields and currents are calculated in magnetic Apex coordinates (Richmond, 1995) using a finer latitudinal grid (~0.5° near the magnetic equator) that is suitable for resolving the EEJ. The TIEGCM simulations are performed for moderate solar activity (F10.7 = 120 sfu, where 1 sfu = 10^{-22} Wm^{-2} Hz^{-1}) and geomagnetically quiet conditions (Kp = 2). We run two simulations: one for 1 January and the other for 1 August, representing two seasonal conditions. Following Fang et al. (2008), the TIEGCM solar fluxes in wavelengths between 8 and 70 Å were multiplied by a factor of 4.4, which gives realistically high E-region conductivities, once it is known that the model underestimates the conductivity values (Doumbia et al., 2007; Fang et al., 2008). The TIEGCM lower boundary was constrained using migrating solar diurnal and semidiurnal tides from the global scale wave model (Hagan & Forbes, 2002, 2003). Tidal forcing at the model lower boundary imitates the effects that tidal waves from the middle and lower atmosphere would have on the ionosphere (Yamazaki & Richmond, 2013). It is noted that tidal forcing used in this study does not include nonmigrating tides (e.g., DE3) or stationary planetary waves that are known to drive the wave-4 longitudinal pattern in the EEJ. The purpose of our TIEGCM experiment is to evaluate the longitudinal variation of the EEJ that results from nonwave-4 sources. Although migrating tidal fields are independent of longitude at a fixed local time, the ionospheric currents driven by migrating tides depend on longitude due to their interaction with the longitudinally varying geomagnetic field. Such an effect was predicted in the study by Doumbia et al. (2007), but the relative importance to the wave-4 is yet to be known. We calculate height-integrated current density J_E in the magnetic eastward direction. To facilitate a direct comparison with the Swarm EEJ data, J_E was separated into a large-scale Sq component and a local EEJ component. The value of the latter component at the magnetic equator gives the predicted EEJ current intensity.

3. Method

The EEJ strength given by ΔH was obtained in two steps. First, for each UT day, the H-component difference between equatorial and low-latitude stations is calculated. Then, the nighttime quiet level is subtracted from the resulting H-component difference, providing the final ΔH. The nighttime quiet level of each night is defined by the average value of the 4 hr around local midnight (Siddiqui et al., 2015). Moreover, ΔH was corrected for noncyclic changes (e.g., Chapman & Bartels, 1940), which were evaluated by linearly interpolating a baseline between successive nighttime quiet levels.

The CEJ events were automatically detected in the 1-min ΔH for each magnetically quiet day. A quiet day was defined when the condition Kp <= 3o lasts for the corresponding LT day but also for 21 LT to 24 LT of the previous day and for 00 LT to 03 LT of the following day.

To identify CEJ events, we used the criterion of $\Delta H < -10$ nT for at least 10 consecutive minutes from 6 LT to 10 LT (for MCEJ) and from 14 LT to 18 LT (for ACEJ). Note that thresholds of $\Delta H < -8$ nT and $\Delta H < -12$ nT give consistent results (not shown here), indicating the robustness of our approach. The MCEJ and ACEJ time intervals chosen here are known to be the periods when CEJs most frequently occur (Marriott et al., 1979; Rastogi, 1974a). We noted a rare occurrence of minima in ΔH around noontime (as also reported by Mayaud, 1977), but such events are not analyzed in this study. Days with data gaps in ΔH exceeding 30 min in the MCEJ and/or ACEJ time intervals were not used for the corresponding period. After considering the quiet days and data gaps constraints, the total number of days used in the MCEJ (ACEJ) analysis for the TTB-KOU and HUA-PIU pairs are 1,838 (1,863) and 1,730 (1,706), respectively.

Our data analysis does not consider possible CEJ variability caused by solar flares. These events are known to affect ionospheric conductivities and, hence, EEJ/CEJ currents. They lead to an amplification of the eastward current during normal EEJ conditions and of the westward current during CEJ conditions (Abdu et al., 2017; Rastogi et al., 1999; Zhang, Liu, Le, Chen, & Kuai, 2017), with very rare exceptions (Rastogi, Chandra, & Yumoto, 2013; Yamazaki et al., 2009). Additionally, it is a solar activity dependent phenomenon which is much more frequent during disturbed periods. Thus, in principle, rapid geomagnetic variations that arise from solar flares do not affect the occurrence rates of quiet-time CEJ and its detection method.

Monthly CEJ occurrence rates were calculated by dividing the number of observed CEJ events by the number of days (without data gaps) that fulfill our criteria for magnetically quiet days. To account for possible solar flux dependencies of monthly CEJ rates, we define two subsets: one for months with low solar flux (mean F10.7 < 96 sfu) and one for months with high solar flux (mean F10.7 > = 96 sfu), where 96 sfu is the median value of the monthly F10.7 averages for the period from June 2008 to December 2017. The average F10.7 value for the subset of low (high) solar flux is 78.0 (126.4) sfu. In the period for which we investigate Swarm data (November 2013 to May 2017), the average F10.7 is 114.4 sfu, closer to the high solar flux subset average. The detected CEJ events are used here to evaluate the CEJ dependence on solar flux, lunar phases, and seasons.

4. Results

4.1. CEJ Annual Rates and Dependence on F10.7

Annual means of F10.7 and CEJ occurrence rates for TTB and HUA were calculated from the monthly values, for the period from June 2008 to December 2017, as shown in Figures 3a and 3b for MCEJ and ACEJ. While MCEJ occurrence rates seem to be independent of F10.7 (correlation coefficients: 0.22 for TTB and 0.30 for HUA), the ACEJ occurrence rates tend to increase for lower F10.7 (correlation coefficients: −0.93 for TTB and −0.73 for HUA). The results at TTB are thus similar to those at other longitudes studied earlier (Marriott et al., 1979; Rastogi, 1974a).

The yearly MCEJ and ACEJ occurrence rates in the Brazilian sector (averaging 62% and 33%, respectively) are constantly higher than in the Peruvian sector (40% and 14%, respectively). The MCEJ rates are notably greater than ACEJ rates in both sectors.

4.2. CEJ Dependence on Lunar Phase

The lunar phase ν varies between 0 and 24 in units of hours, where ν = 0 and ν = 12 represent new and full moon, respectively. For each hour of ν, the occurrence rate of MCEJ and ACEJ was calculated by dividing the

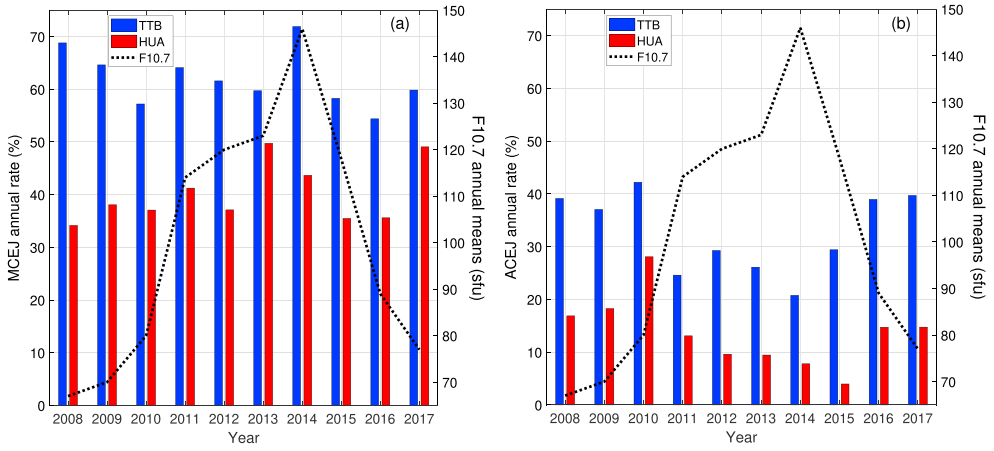

Figure 3. F10.7 annual means (black-dashed line) and TTB (blue bars) and HUA (red bars) annual occurrence rates of MCEJ (a) and ACEJ (b) for June 2008 to December 2017. TTB = Tatuoca; HUA = Huancayo; MCEJ = morning counter electrojet; ACEJ = afternoon counter electrojet.

number of detected events by the number of quiet, gap-free days. The value of ν was calculated for each day according to the formula $\nu = \lambda_M - \lambda_S$, from Sugiura and Fanselau (1966), where λ_M and λ_S are the mean longitudes of the moon and sun, respectively, given by equations (1) and (2):

$$\lambda_M = 283.612983° + 13.176396730246°t_d + 0.00198°T^2, \quad (1)$$

$$\lambda_S = 280.682325° + 0.985647335387°t_d + 0.00030°T^2. \quad (2)$$

Here time t_d is expressed in number of days since 12-hr Greenwich Mean Time on 1 January 1900, and T is the same time measured in units of Julian centuries (equal to 36,525 days).

The MCEJ and ACEJ dependence on the lunar phase is presented in Figures 4a and 4b. The effect of the semi-monthly lunar tide is clear in both cases, and it is very similar in TTB and HUA with a variability of around 40% for MCEJ and 20% for ACEJ occurrences. A phase shift between MCEJ and ACEJ peak occurrences characterizes the results: while MCEJ events are more frequent around 6 and 18 hr (i.e., first and third quarters of the moon), ACEJ events are more frequent around 0 and 12 hr (i.e., new and full moons). Our results suggest that the CEJ occurrence rate at TTB is strongly influenced by the lunar tide in a similar way as at HUA.

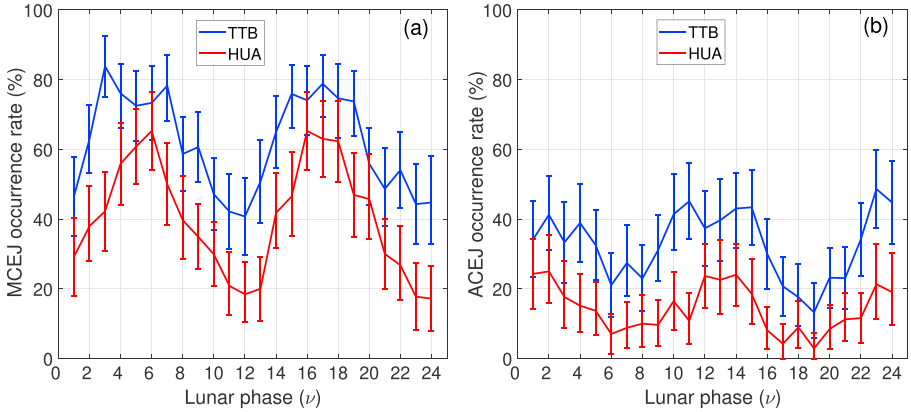

Figure 4. Dependence of MCEJ (a) and ACEJ (b) occurrence rates on lunar phase at TTB (blue) and HUA (red). Error bars represent the 95% confidence interval, calculated by the bootstrap technique (Efron, 1981). TTB = Tatuoca; HUA = Huancayo; MCEJ = morning counter electrojet; ACEJ = afternoon counter electrojet.

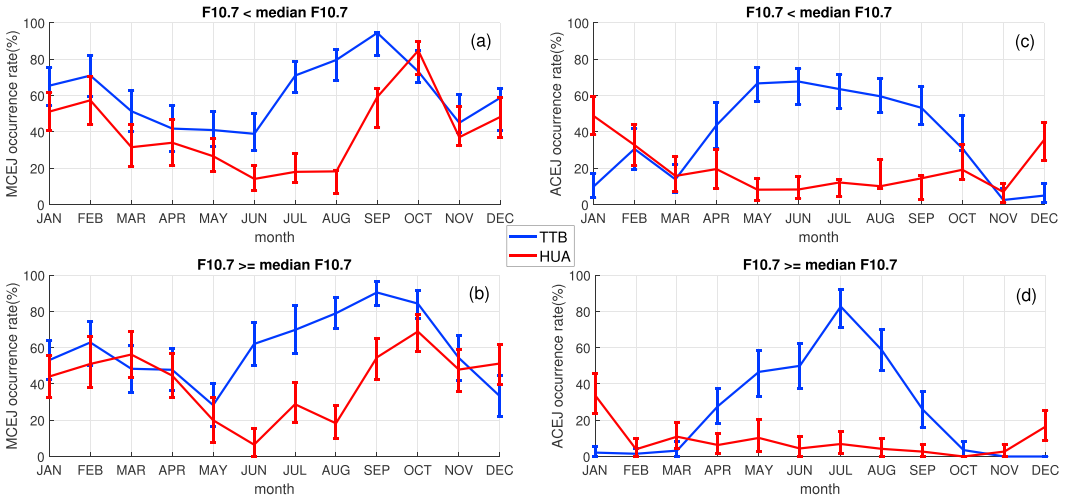

Figure 5. Monthly MCEJ (a and b) and ACEJ (c and d) occurrence rates for TTB (blue) and HUA (red), for low (a and c) and high (b and d) solar flux conditions. Error bars represent the 95% confidence interval, calculated by the bootstrap technique. TTB = Tatuoca; HUA = Huancayo; MCEJ = morning counter electrojet; ACEJ = afternoon counter electrojet.

4.3. Seasonal Dependence of CEJ

The monthly MCEJ and ACEJ occurrence rates detected for TTB and HUA are shown in Figure 5 for low and high F10.7 conditions. For both solar flux levels, the TTB and HUA MCEJ occurrence rates are similar from October to May, but they are significantly larger at TTB for June to September (Figures 5a and 5b). For both solar flux levels, the ACEJ occurrence rates (Figures 5c and 5d) are larger at TTB from April to October, while they are larger at HUA from November to March. Note that for both MCEJ and ACEJ occurrence rates, the differences between TTB and HUA are the largest around July–August. The seasonal pattern of CEJ occurrence rates does not strongly depend on solar flux level, and the main features described above are present in both the low and the high solar flux subsets.

4.4. Seasonal Analysis of Swarm Data

The satellite-derived EEJ current intensity (in milliampere per meter) was analyzed separately for the intervals 6 LT to 10 LT and 14 LT to 18 LT. The seasonal and longitudinal dependence was determined by binning the data within a 30° longitude window into 3-month bins.

Figures 6a and 6b shows the seasonal and longitudinal variabilities of CEJ occurrence rates for morning and afternoon periods, respectively. Here CEJ events were detected as westward current occasions (negative values in the current intensity). A sharp gradient in CEJ occurrence rates is seen between TTB and HUA longitudes (−48° and −75°, indicated by blue and red triangles, respectively). This gradient is part of a wave-4 longitudinal structure, which is most evident from April to October.

The average EEJ intensity is shown in Figures 6c and 6d for morning and afternoon. A comparison between Figures 6a and 6c, as well as between Figures 6b and 6d, shows that the occurrence rate of CEJ and the average EEJ intensity are strongly anticorrelated. Therefore, understanding the seasonal and longitudinal climatology of the average EEJ is equivalent to understanding the seasonal and longitudinal climatology of CEJ occurrence rate.

The inverse relationship between the CEJ occurrence rate and average EEJ intensity at TTB and HUA longitudes is also obvious in Figures 7a and 7c, for morning hours, and in Figures 7b and 7d, for afternoon hours. In the morning, the EEJ is stronger at HUA throughout the year, while in the afternoon, the EEJ is stronger in the Brazilian sector between December and February. The results indicate a stronger dependence on season at TTB than at HUA.

The seasonal variation of the CEJ occurrence rate for TTB and HUA longitudes derived from Swarm data is in agreement with the results obtained from ground-based records presented in section 4.3, with maximum differences between Brazilian and Peruvian sectors around July–August.

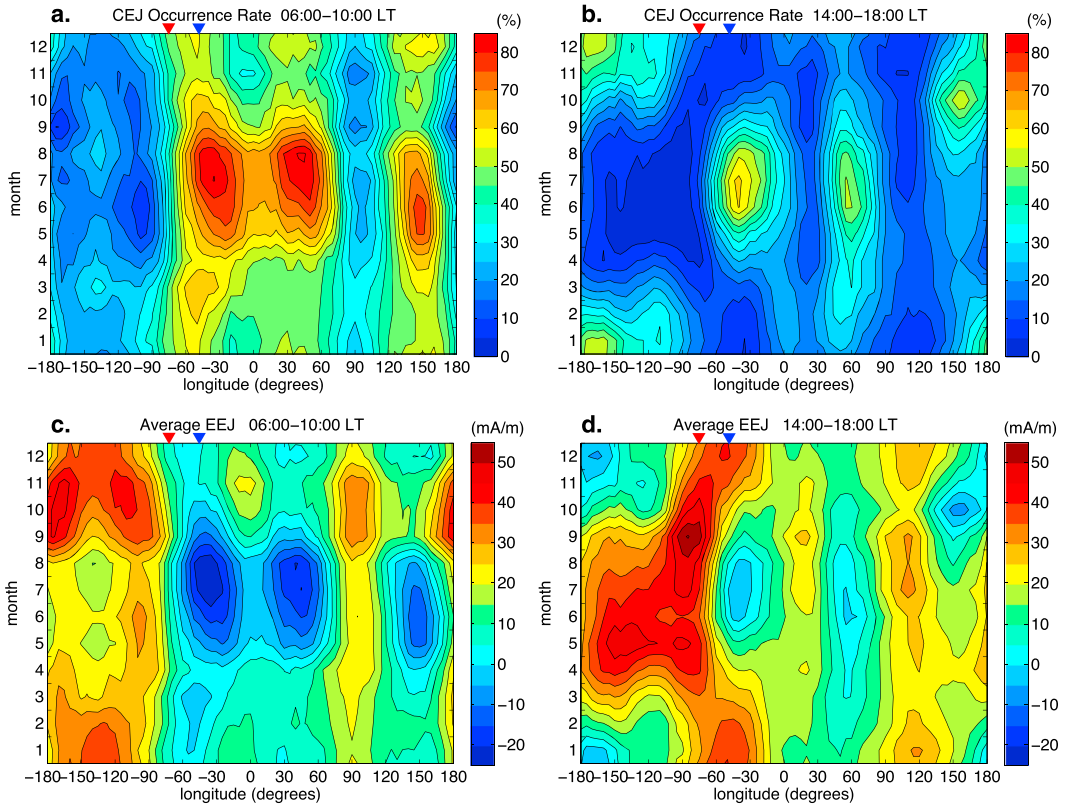

Figure 6. Longitudinal and seasonal variability of morning CEJ (a) and afternoon CEJ (b) occurrence rates (in %) and of average EEJ intensity (in mA/m) for morning (c) and afternoon (d), derived from Swarm measurements. Tatuoca and Huancayo longitudes are indicated by blue and red triangles, respectively. CEJ = counter electrojet; EEJ = equatorial electrojet.

The average EEJ intensity in the morning and afternoon (Figures 7e and 7f) shows a wave-4 longitudinal pattern for July–August (black solid line) and a different pattern for December–January (gray-dashed line). During July–August, both morning and afternoon average EEJ intensities present a sharp gradient between TTB (blue vertical line) and HUA (red vertical line) longitudes. For December–January, their strength is comparable.

5. Discussion

While the review by Mayaud (1977) reports that, globally, ACEJ events are much more frequent than MCEJ events, we find significantly more MCEJ than ACEJ events for the American sector. This could be explained by the different CEJ detection methods or the different observations periods used in our work and in the studies presented by Mayaud (1977), which can be found in Onwumechili and Akasofu (1972), Rastogi (1974a), and Marriott et al. (1979). Concerning the used methods, all these studies relied their CEJ detection on the analysis of isolated H-component depressions below the nighttime base level (and not on station pair difference). From these, Marriott et al. (1979) is the only study that considered a CEJ intensity threshold, requiring a depression of at least −15 nT. Furthermore, Onwumechili and Akasofu (1972) and Marriott et al. (1979) considered magnetically quiet conditions based on different Kp index constraints, whereas Rastogi (1974a) defined quiet day patterns after visual examination of magnetograms. However, more recently, Patil et al. (1990a, 1990b) and Rabiu et al. (2017) also reported a predominance of MCEJ for HUA. Regarding the Brazilian sector, our observed MCEJ predominance is in agreement with Venkatesh et al. (2015), who found that 75% of the CEJ events occur before 10 LT.

The observed anticorrelation of ACEJ at TTB with solar flux (Figure 3b) agrees with previous results for HUA (Marriott et al., 1979; Rastogi, 1974a).

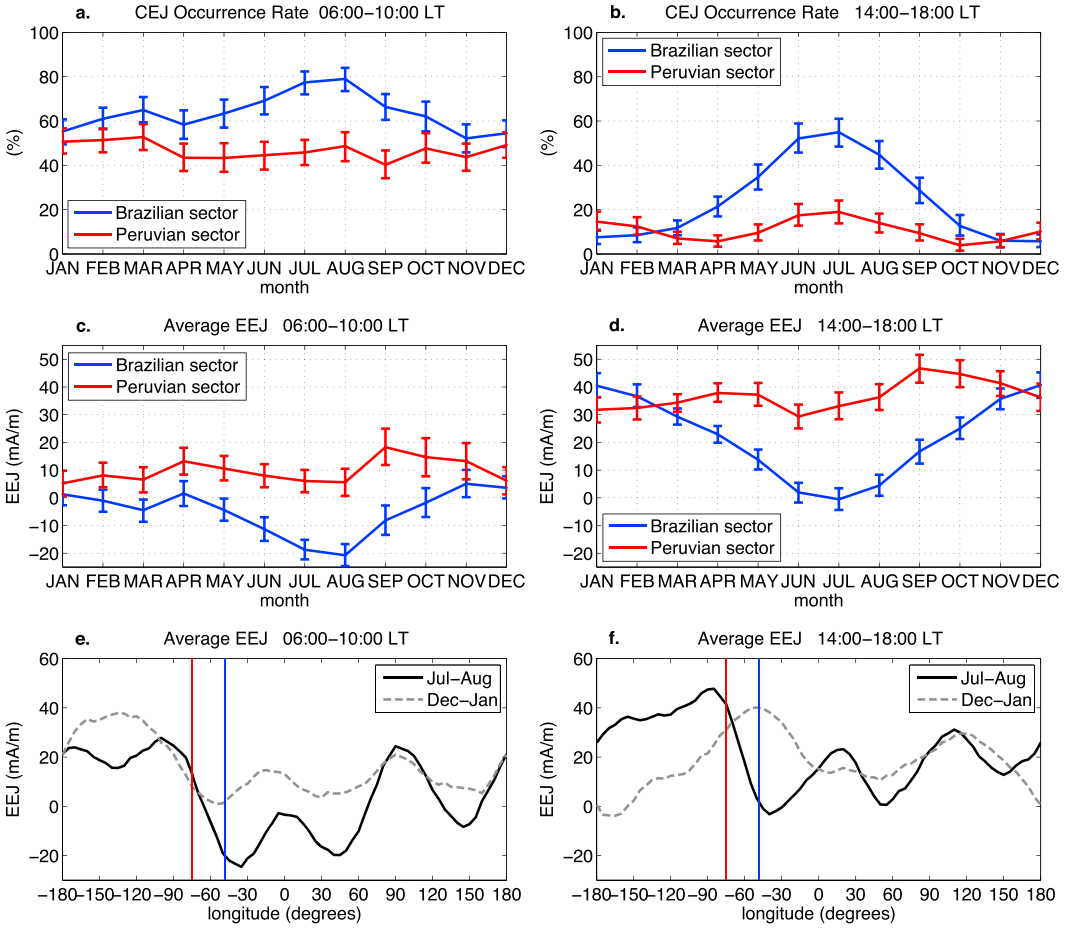

Figure 7. CEJ occurrence rate (in %) and average EEJ intensity (in mA/m) obtained from Swarm measurements for the Brazilian (blue) and Peruvian (red) sectors, during morning (a and c) and afternoon (b and d). (e) and (f) show the longitudinal climatology of the EEJ (in mA/m) for July–August (solid black line) and for December–January (gray-dashed line). Tatuoca and Huancayo longitudes are indicated by vertical blue and red lines, respectively. Error bars represent the 95% confidence interval, calculated by the bootstrap technique. CEJ = counter electrojet; EEJ = equatorial electrojet.

The results obtained for the CEJ dependence on lunar phase (Figure 4) are also in agreement with previous studies. Rastogi (1974b), Marriott et al. (1979), and Patil et al. (1990a) analyzed HUA data from 1948 to 1971, 1922 to 1967, and 1964 to 1965, respectively, and their results are consistent with the MCEJ peaks of occurrence during the first and third quarters of the moon and ACEJ peaks during new and full moons found in this work. The phase of the semimonthly lunar variation is known to change with solar time, which explains the time shift between MCEJ and ACEJ lunar modulations. The observed different peak-to-peak lunar tide modulation amplitudes for MCEJ and ACEJ seen in Figures 4a and 4b are probably a consequence of the prenoon M_2 lunar tide peak (proportional to ΔH, which also peaks before noon), as shown by Rastogi and Trivedi (1970). This leads to greater lunar tide amplitudes for morning periods and, hence, MCEJ oscillations.

The HUA CEJ seasonal climatology presented in Figure 5 follows the trends observed in the CEJ analysis of Marriott et al. (1979), Patil et al. (1990a), and Rabiu et al. (2017), although different CEJ detection techniques were adopted in each work. Shume et al. (2010) pointed out the difference in the seasonal variations of the EEJ intensity between the Peruvian and Brazilian sectors. They showed that the EEJ intensity exhibits a semiannual variation with equinoctial maxima in the Peruvian sector, while the EEJ intensity peaks during the northern-hemisphere winter in the Brazilian sector, which is in agreement with our results presented in Figures 7c and 7d. Yizengaw et al. (2014) suggested an average pattern of the EEJ seasonal variability with higher magnitudes during equinoxes and lower magnitudes in the June solstice. This pattern is consistent

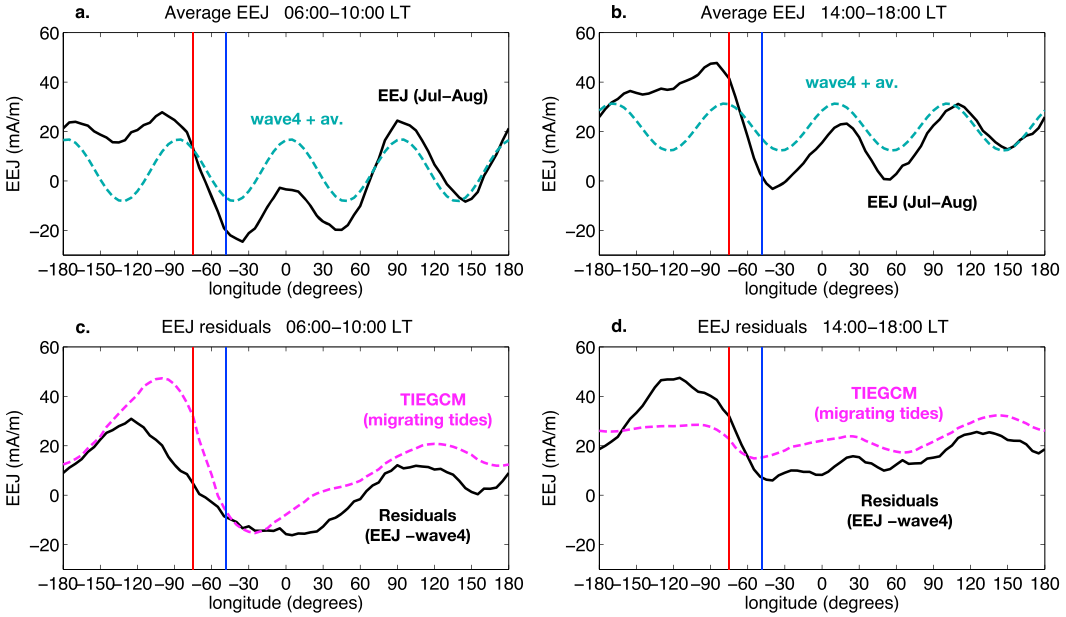

Figure 8. Average EEJ intensity derived from Swarm (for July–August, black solid line) and wave-4 fits plus an average of the corresponding EEJ data (green-dashed line) for morning (a) and afternoon (b). Residuals (EEJ minus wave-4, black solid line) and TIEGCM simulation results for August (magenta-dashed line) for morning (c) and afternoon (d). The Brazilian (Tatuoca) and Peruvian (Huancayo) longitudes are indicated by blue and red vertical lines, respectively. CEJ = counter electrojet; EEJ = equatorial electrojet; TIEGCM = Thermosphere-Ionosphere-Electrodynamics General Circulation Model.

with our HUA results, but in TTB longitude, during the afternoon period, the EEJ intensity presents higher magnitudes during the December solstice (Figures 7c and 7d).

Despite some differences between the CEJ occurrence rates derived from the ground (Figure 5) and Swarm (Figures 7a and 7b) measurements, the two results are in qualitative agreement: the maximum difference between the Brazilian and Peruvian sectors (for both morning and afternoon periods) occurs around July–August, when the wave-4 pattern dominates.

Singh et al. (2018) showed that the DE3 tide gives rise to the wave-4 longitudinal pattern in the occurrence rate of ACEJ. Our results suggest that the wave-4 longitudinal pattern is also an important source of longitudinal variability for the MCEJ occurrence rate. Neither MCEJ nor ACEJ occurrence rates reveal the wave-4 pattern during December–January (Figures 7e and 7f, gray-dashed lines). It is not yet well established what mechanism dominates the longitudinal variability of the EEJ during the northern-hemisphere winter (see Lühr & Manoj, 2013, for more discussion).

As pointed out by Lühr et al. (2008), the longitudinal variation of the EEJ intensity cannot be fully explained by the wave-4 associated with DE3 even during the northern-hemisphere summer. We show this by subtracting a fit of a wave-4 curve in the form $A\cos(4\lambda - \Phi)$ from the EEJ intensity derived from the Swarm measurements, where λ is the longitude, and A and Φ are the amplitude and phase of the wave-4 curve that can be determined using the least-squares method. In Figures 8a and 8b, the black lines show the Swarm EEJ data (for July–August period), while the green-dashed lines show the wave-4 fit (offset by the average value of the corresponding data). The blue and red vertical lines indicate TTB and HUA longitudes, respectively. The wave-4 fits reproduce the longitudinal variability of the EEJ intensity to a good extent. These fits can be considered to represent the effect of DE3 along with other nonmigrating tides and stationary planetary waves that are known to contribute to the wave-4 longitudinal structure (e.g., Pedatella et al., 2012). It can be seen in Figures 8a and 8b that the longitudinal variation due to the wave-4 structure can explain 10–20 mA/m in the longitudinal difference of the EEJ intensity between TTB and HUA.

The residuals from the wave-4 fits (Swarm EEJ minus wave-4) are plotted in Figures 8c and 8d (black lines), representing the contribution due to other sources than wave-4. The longitudinal difference in the EEJ intensity between TTB and HUA is as large as 10–20 mA/m in the residuals. This means that the wave-4

longitudinal structure accounts for about half of the longitudinal difference of the EEJ intensity between TTB and HUA, and the rest should be attributed to other mechanisms.

The magenta-dashed lines in Figures 8c and 8d show the TIEGCM results. The simulation produced very similar results for January and August, and we therefore show only the results for August. The model reproduces the main longitudinal pattern of the EEJ residuals. Agreement is good in both morning and afternoon hours. It is noted that our TIEGCM simulation takes into account the effect of migrating tides only, without nonmigrating tides and stationary planetary waves that produce longitudinally dependent structures (like the wave-4). Thus, the results suggest a significant longitudinal modulation of the EEJ intensity by migrating tides.

It is true that neutral wind oscillations due to migrating tides do not depend on longitude when considering a fixed local time. Nonetheless, the longitudinal variation of the EEJ occurs in the TIEGCM driven by migrating tides. This is because the model uses a realistic geomagnetic main field distribution from the IGRF model (see Thébault et al., 2015, for its most recent version) that varies with longitude. In addition, longitudinal changes in the geomagnetic main field are particularly strong in the South American sector due to the South Atlantic Magnetic Anomaly.

The intensity of the geomagnetic main field affects the ionospheric electrodynamics (thus EEJ) by modulating ionospheric conductivities and dynamo electric field (a similar effect was observed in long-term observations at HUA due to secular variation; Matzka et al., 2017). Doumbia et al. (2007) noted this effect in the EEJ simulated by the TIEGCM and referred to it as IGRF effect. The EEJ minus wave-4 residuals presented in Figures 8c and 8d can be explained by a coupling effect of migrating tidal winds and inhomogeneous geomagnetic main field. Doumbia et al. (2007) also noted that TIEGCM simulations considering only migrating tides can reproduce CEJ occurrences in the Brazilian sector (longitude $-55°$ in their Figures 5 and 10). However, they were unaware that nonmigrating tides and stationary planetary waves can also contribute to the CEJ occurrence in the Brazilian sector.

Finally, we would like to emphasize that the observed sharp gradient of the EEJ intensity between the Brazilian and Peruvian sectors during the northern-hemisphere summer arises from both the wave-4 longitudinal structure (Figures 8a and 8b) and the effect of migrating tides (Figures 8c and 8d). These two mechanisms are adding (by similar order of milliampere per meter) to the observed longitudinal variability of the EEJ and CEJ in the American sector.

6. Conclusions

We have examined for the first time the CEJ climatology and dependence on solar flux and lunar phase in the Brazilian sector by using 10 years of ground-based magnetometer data. The occurrence rate of CEJ events at TTB has been shown to depend on season, solar flux, and lunar phase. Characteristics of the CEJ climatology in the Brazilian sector are compared with those in the Peruvian sector at HUA as well as with previous results in the literature. The main findings of this work are the following:

1. The occurrence rate of CEJ is generally higher at TTB than at HUA. The solar flux and lunar phase modulation of the CEJ occurrence rate at TTB is similar to that at HUA. A predominance of MCEJ events is observed at both TTB and HUA.
2. There is a significant difference in the occurrence rate of CEJ between TTB and HUA during the northern-hemisphere summer months.
3. During the northern-hemisphere summer months, the average EEJ is much weaker in the Brazilian sector than in the Peruvian sector. The EEJ intensity sharply decreases from 90°W to 40°W, and the global analysis of Swarm data suggest that this longitudinal gradient is partly due to the wave-4 longitudinal structure arising from nonmigrating tides and stationary planetary waves. The wave-4 effect is found not only in ACEJ, as recently reported by Singh et al. (2018), but also in MCEJ.
4. TIEGCM results suggest that the longitudinal variation of the EEJ intensity resulting from migrating tides also makes a contribution to the observed longitudinal gradient of the EEJ intensity over the American sector. Both the effects of migrating tides (across the longitudinally varying geomagnetic main field) and wave-4 pattern are of similar size and, combined, lead to a stronger EEJ in the Peruvian sector than in the Brazilian sector during the northern-hemisphere summer, resulting in higher CEJ occurrence rates in the Brazilian sector.

Acknowledgments
The results presented in this paper rely on the data collected at HUA and KOU. We thank Instituto Geofísico del Perú and Institut de Physique du Globe de Paris for supporting HUA and KOU operation, respectively, and INTERMAGNET for promoting high standards of geomagnetic observatory practice (www.intermagnet.org). We acknowledge LISN network for operating PIU. TTB is maintained and operated by Observatório Nacional and GFZ German Research Centre for Geosciences (data available at http://dataservices.gfz-potsdam.de/portal/). The Swarm satellite mission is operated by ESA, and its data are available at https://earth.esa.int/swarm. GFZ German Research Centre for Geosciences provides the geomagnetic Kp index, and Natural Resources Canada provides F10.7 solar flux data. Annual means of TTB and HUA geomagnetic data used in Figure 1b were obtained from the World Data Centre for Geomagnetism Edinburgh (http://wdc.bgs.ac.uk/). G. B. S. was supported by MSc and PhD research grants from The National Council for Scientific and Technological Development (CNPq/Brazil, grant 131585/2017-7), FAPERJ (grant E-26/200.632/2018), and CAPES (grant 1799579). Y. Y. was supported by the Humboldt Research Fellowship for Experienced Researchers from the Alexander von Humboldt Foundation. J. M. and C. S. were supported by DFG through its priority program SPP 1788 "Dynamic Earth." K. P. was supported by The National Council for Scientific and Technological Development (CNPq/Brazil, grant 309884/2016-0) and FAPERJ (grant E-26/202.830/2015).

References

Abdu, M. A., Nogueira, P. A. B., Souza, J. R., Batista, I. S., Dutra, S. L. G., & Sobral, J. H. A. (2017). Equatorial electrojet responses to intense solar flares under geomagnetic disturbance time electric fields. *Journal of Geophysical Research: Space Physics*, *122*, 3570–3585. https://doi.org/10.1002/2016JA023667

Alken, P., Maus, S., Chulliat, A., Vigneron, P., Sirol, O., & Hulot, G. (2015). Swarm equatorial electric field chain: First results. *Geophysical Research Letters*, *42*, 673–680. https://doi.org/10.1002/2014GL062658

Alken, P., Maus, S., Vigneron, P., Sirol, O., & Hulot, G. (2013). Swarm SCARF equatorial electric field inversion chain. *Earth, Planets and Space*, *65*(11), 1309–1317. https://doi.org/10.5047/eps.2013.09.008

Anandarao, B. G. (1976). Effects of gravity wave winds and wind shears on equatorial electrojet. *Geophysical Research Letters*, *3*(9), 545–548. https://doi.org/10.1029/GL003i009p00545

Anderson, D., Anghel, A., Chau, J. L., & Yumoto, K. (2006). Global, low-latitude, vertical E×B drift velocities inferred from daytime magnetometer observations. *Space Weather*, *4*, S08003. https://doi.org/doi:10.1029/2005SW000193

Archana, R. K., Chandrasekhar, N. P., Arora, K., & Nagarajan, N. (2018). Constraints on scale lengths of equatorial electrojet and counter electrojet phenomena from the Indian sector. *Journal of Geophysical Research: Space Physics*, *123*, 6821–6835.. https://doi.org/10.1029/2018JA025213

Chapman, S. (1951). The equatorial electrojet as detected from the abnormal electric current distribution about Huancayo, Peru and elsewhere. *Archiv fur Meteorologie, Geophysik, und Bioklimatologie Serie A Meteorologie und Geophysik*, *4*(1), 368–390. https://doi.org/10.1007/BF02246814

Chapman, S., & Bartels, J. (1940). *Geomagnetism*. London, U. K: Oxford University Press.

Chulliat, A., Matzka, J., Masson, A., & Milan, S. (2016). Key ground-based and space-based assets to disentangle magnetic field sources in the Earth's environment. *Space Science Reviews*, *206*(1-4), 123–156. https://doi.org/10.1007/s11214-016-0291-y

Denardini, C. M., Abdu, M. A., Aveiro, H. C., Resende, L. C. A., Almeida, P. D. S. C., Olivio, E. P. A., et al. (2009). Counter electrojet features in the Brazilian sector: Simultaneous observation by radar, digital sounder and magnetometers. *Annales Geophysicae*, *27*(4), 1593–1603. https://doi.org/10.5194/angeo-27-1593-2009

Doumbia, V., Maute, A., & Richmond, A. D. (2007). Simulation of equatorial electrojet magnetic effects with the Thermosphere-Ionosphere-Electrodynamics General Circulation Model. *Journal of Geophysical Research*, *112*, A09309. https://doi.org/10.1029/2007JA012308

Doumouya, V., Vassal, J., Cohen, Y., Fambitakoye, O., & Menvielle, M. (1998). Equatorial electrojet at African longitudes: First results from magnetic measurements. *Annales Geophysicae*, *16*(6), 658–666. https://doi.org/10.1007/s00585-998-0658-9

Efron, B. (1981). Nonparametric estimates of standard error: The jackknife, the bootstrap, and other methods. *Biometrika*, *68*(3), 589–599. https://doi.org/10.1093/biomet/68.3.589

Emmert, J. T., Richmond, A. D., & Drob, D. P. (2010). A computationally compact representation of magnetic-apex and quasi-dipole coordinates with smooth base vectors. *Journal of Geophysical Research*, *115*, A08322. https://doi.org/10.1029/2010JA015326

England, S. L., Maus, S., Immel, T. J., & Mende, S. B. (2006). Longitudinal variation of the E region electric fields caused by atmospheric tides. *Geophysical Research Letters*, *33*, L21105. https://doi.org/10.1029/2006GL027465

Fang, T.-W., Fuller-Rowell, T., Wang, H., Akmaev, R., & Wu, F. (2014). Ionospheric response to sudden stratospheric warming events at low and high solar activity. *Journal of Geophysical Research: Space Physics*, *119*, 7858–7869. https://doi.org/10.1002/2014JA020142

Fang, T. -W., Richmond, A. D., Liu, J. Y., Maute, A., Lin, C. H., Chen, C. H., & Harper, B. (2008). Model simulation of the equatorial electrojet in the Peruvian and Philippine sectors. *Journal of Atmospheric and Solar-Terrestrial Physics*, *70*(17), 2203–2211. https://doi.org/10.1016/j.jastp.2008.04.021

Fejer, B. G., Jensen, J. W., & Su, S. Y. (2008). Quiet time equatorial F region vertical plasma drift model derived from ROCSAT-1 observations. *Journal of Geophysical Research*, *113*, A05304. https://doi.org/10.1029/2007JA012801

Fejer, B. G., Olson, M. E., Chau, J. L., Stolle, C., Lühr, H., Goncharenko, L. P., et al. (2010). Lunar-dependent equatorial ionospheric electrodynamic effects during sudden stratospheric warmings. *Journal of Geophysical Research*, *115*, A00G03. https://doi.org/10.1029/2010JA015273

Friis-Christensen, E., Luhr, H., & Hulot, G. (2006). Swarm: A constellation to study the Earth's magnetic field. *Earth, Planets and Space*, *58*(4), 351–358. https://doi.org/10.1186/BF03351933

Friis-Christensen, E., Luhr, H., Knudsen, D., & Haagmans, R. (2008). Swarm—An Earth observation mission investigating geospace. *Advances in Space Research*, *41*(1), 210–216. https://doi.org/10.1016/j.asr.2006.10.008

Gouin, P., & Mayaud, P. N. (1967). A propos de lexistence possible d'un "contre-electrojet" aux latitudes magnetiques equatoriales. *Annales de Géophysique*, *23*, 41–47.

Gurubaran, S. (2002). The equatorial counter electrojet: Part of a worldwide current system? *Geophysical Research Letters*, *29*(9), 1337. https://doi.org/10.1029/2001GL014519

Hagan, M. E., & Forbes, J. M. (2002). Migrating and nonmigrating diurnal tides in the middle and upper atmosphere excited by tropospheric latent heat release. *Journal of Geophysical Research*, *107*(D24), 4754. https://doi.org/10.1029/2001JD001236

Hagan, M. E., & Forbes, J. M. (2003). Migrating and nonmigrating semidiurnal tides in the upper atmosphere excited by tropospheric latent heat release. *Journal of Geophysical Research*, *108*(A2), 1062. https://doi.org/10.1029/2002JA009466

Hagan, M. E., Maute, A., Roble, R. G., Richmond, A. D., Immel, T. J., & England, S. L. (2007). Connections between deep tropical clouds and the Earth's ionosphere. *Geophysical Research Letters*, *34*, L20109. https://doi.org/10.1029/2007GL030142

Hanuise, C., Mazaudier, C., Vila, P., Blanc, M., & Crochet, M. (1983). Global dynamo simulation of ionospheric currents and their connection with the equatorial electrojet and counter electrojet: A case study. *Journal of Geophysical Research*, *88*(A1), 253–270. https://doi.org/10.1029/JA088iA01p00253

Immel, T. J., Sagawa, E., England, S. L., Henderson, S. B., Hagan, M. E., Mende, S. B., et al. (2006). Control of equatorial ionospheric morphology by atmospheric tides. *Geophysical Research Letters*, *33*, L15108. https://doi.org/10.1029/2006GL026161

Kane, R. P., & Trivedi, N. B. (1981). Confinement of equatorial counter electrojets to restricted longitudes. *Journal of Geomagnetism and Geoelectricity*, *33*(6), 379–382. https://doi.org/10.5636/jgg.33.379

Kane, R. P., & Trivedi, N. B. (1982). Comparison of equatorial electrojet characteristics at Huancayo and Eusebio (Fortaleza) in the South American region. *Journal of Atmospheric and Solar-Terrestrial Physics*, *44*(9), 785–792. https://doi.org/10.1016/0021-9169(82)90007-1

Kikuchi, T., Hashimoto, K. K., Kitamura, T.-I., Tachihara, H., & Fejer, B. (2003). Equatorial counterelectrojets during substorms. *Journal of Geophysical Research*, *108*(A11), 1406. https://doi.org/10.1029/2003JA009915

Kikuchi, T., Hashimoto, K. K., & Nozaki, K. (2008). Penetration of magnetospheric electric fields to the equator during a geomagnetic storm. *Journal of Geophysical Research*, *113*, A06214. https://doi.org/10.1029/2007JA012628

Kil, H., Oh, S. -J., Kelley, M. C., Paxton, L. J., England, S. L., Talaat, E., et al. (2007). Longitudinal structure of the vertical E ×B drift and ion density seen from ROCSAT-1. *Geophysical Research Letters*, *34*, L14110. https://doi.org/10.1029/2007GL030018

Lühr, H., & Manoj, C. (2013). The complete spectrum of the equatorial electrojet related to solar tides: CHAMP observations. *Annales Geophysicae*, *31*(8), 1315–1331. https://doi.org/10.5194/angeo-31-1315-2013

Lühr, H., Rother, M., Hausler, K., Alken, P., & Maus, S. (2008). The influence of nonmigrating tides on the longitudinal variation of the equatorial electrojet. *Journal of Geophysical Research*, *113*, A08313. https://doi.org/10.1029/2008JA013064

Marriott, R. T., Richmond, A. D., & Venkateswaran, S. V. (1979). The quiet-time equatorial electrojet and counter-electrojet. *Journal of Geomagnetism and Geoelectricity*, *31*(3), 311–340. https://doi.org/10.5636/jgg.31.311

Matzka, J., Chulliat, A., Mandea, M., Finlay, C. C., & Qamili, E. (2010). Geomagnetic observations for main field studies: From ground to space. *Space Science Reviews*, *155*(1-4), 29–64. https://doi.org/10.1007/s11214-010-9693-4

Matzka, J., Siddiqui, T. A., Lilienkamp, H., Stolle, C., & Veliz, O. (2017). Quantifying solar flux and geomagnetic main field influence on the equatorial ionospheric current system at the geomagnetic observatory Huancayo. *Journal of Atmospheric and Solar-Terrestrial Physics*, *163*, 120–125. https://doi.org/10.1016/j.jastp.2017.04.014

Mayaud, P. N. (1977). The equatorial counter-electrojet—A review of its geomagnetic aspects. *Journal of Atmospheric and Solar-Terrestrial Physics*, *39*(9-10), 1055–1070. https://doi.org/10.1016/0021-9169(77)90014-9

Morschhauser, A., Soares, G. B., Haseloff, J., Bronkalla, O., Protásio, J., Pinheiro, K., & Matzka, J. (2017). The geomagnetic observatory on Tatuoca Island, Brazil: History and recent developments. *Geoscientific Instrumentation, Methods and Data Systems*, *6*(2), 367–376. https://doi.org/10.5194/gi-6-367-2017

Oberheide, J., Forbes, J. M., Häusler, K., Wu, Q., & Bruinsma, S. L. (2009). Tropospheric tides from 80 to 400 km: Propagation, interannual variability, and solar cycle effects. *Journal of Geophysical Research*, *114*, D00I05. https://doi.org/10.1029/2009JD012388

Onwumechili, A., & Akasofu, S. I. (1972). On the abnormal depression of Sq(H) under the equatorial electrojet in the afternoon. *Journal of Geomagnetism and Geoelectricity*, *24*(2), 161–173. https://doi.org/10.5636/jgg.24.161

Pandey, K., Sekar, R., Anandarao, B. G., Gupta, S. P., & Chakrabarty, D. (2018). On the occurrence of afternoon counter electrojet over Indian longitudes during June solstice in solar minimum. *Journal of Geophysical Research: Space Physics*, *123*, 2204–2214. https://doi.org/10.1002/2017JA024725

Patil, A. R., Rao, D. R. K., & Rastogi, R. G. (1990a). Equatorial electrojet strengths in the Indian and American sectors part I. during low solar activity. *Journal of Geomagnetism and Geoelectricity*, *42*(7), 801–811. https://doi.org/10.5636/jgg.42.801

Patil, A. R., Rao, D. R. K., & Rastogi, R. G. (1990b). Equatorial electrojet strengths in the Indian and American sectors part II. During high solar activity. *Journal of Geomagnetism and Geoelectricity*, *42*(7), 813–823. https://doi.org/10.5636/jgg.42.813

Pedatella, N. M., Hagan, M. E., & Maute, A. (2012). The comparative importance of DE3, SE2, and SPW4 on the generation of wavenumber-4 longitude structures in the low-latitude ionosphere during September equinox. *Geophysical Research Letters*, *39*, L19108. https://doi.org/10.1029/2012GL053643

Pfaff, R. F. Jr., Acuña, M. H., Marionni, P. A., & Trivedi, N. B. (1997). DC polarization electric field, current density, and plasma density measurements in the daytime equatorial electrojet. *Geophysical Research Letters*, *24*, 1667–1670.

Qian, L., Burns, A. G., Emery, B. A., Foster, B., Lu, G., Maute, A., et al. (2014). The NCAR TIE-GCM. In J. Huba, R. Schunk, & G. Khazanov (Eds.), *Modeling the ionosphere-thermosphere system* (pp. 73–83). Chichester: Wiley. https://doi.org/10.1002/9781118704417.ch7

Rabiu, A. B., Folarin, O. O., Uozumi, T., Abdul Hamid, N. S., & Yoshikawa, A. (2017). Longitudinal variation of equatorial electrojet and the occurrence of its counter electrojet. *Annales Geophysicae*, *35*(3), 535–545. https://doi.org/10.5194/angeo-35-535-2017

Rastogi, R. G. (1974a). Westward equatorial electrojet during daytime hours. *Journal of Geophysical Research*, *79*(10), 1503–1512. https://doi.org/10.1029/JA079i010p01503

Rastogi, R. G. (1974b). Lunar effects in the counter electrojet near the magnetic equator. *Journal of Atmospheric and Solar-Terrestrial Physics*, *36*(1), 167–170. https://doi.org/10.1016/0021-9169(74)90074-9

Rastogi, R. G. (1977). Geomagnetic storms and electric fields in the equatorial ionosphere. *Nature*, *268*(5619), 422–424. https://doi.org/10.1038/268422a0

Rastogi, R. G., Chandra, H., Janardhan, P., & Rahul, S. (2014). Equatorial and midlatitude ionospheric currents over the Indian region based on 40 years of data at Trivandrum and Alibag. *Indian Journal of Radio & Space Physics*, *43*, 274–283

Rastogi, R. G., Chandra, H., Rahul, S., Trivedi, N. B., & Fontes, S. L. (2013). A comparison of equatorial electrojet in Peru and East Brazil. *The Open Atmospheric Science Journal*, *7*(1), 29–36, https://doi.org/10.2174/1874282320130417003

Rastogi, R. G., Chandra, H., & Yumoto, K. (2013). Unique examples of solar flare effects in geomagnetic H field during partial counter electrojet along CPMN longitude sector. *Earth, Planets and Space*, *65*(9), 1027–1040. https://doi.org/10.5047/eps.2013.04.004

Rastogi, R. G., Pathan, B. M., Rao, D. R. K., Sastry, T. S., & Sastri, J. H. (1999). Solar flare effects on the geomagnetic elements during normal and counter electrojet periods. *Earth, Planets and Space*, *51*(9), 947–957. https://doi.org/10.1186/BF03351565

Rastogi, R. G., & Trivedi, N. B. (1970). Luni-solar tides in H at stations within the equatorial electrojet. *Planetary and Space Science*, *18*(3), 367–377. https://doi.org/10.1016/0032-0633(70)90174-1

Rastogi, R. G., & Yumoto, K. (2006). Equatorial electrojet in the East Brazil anomaly region. *Earth, Planets and Space*, *58*, 103–106.

Richmond, A. D. (1995). Ionospheric electrodynamics using magnetic apex coordinates. *Journal of Geomagnetism and Geoelectricity*, *47*(2), 191–212. https://doi.org/10.5636/jgg.47.191

Richmond, A. D., Ridley, E. C., & Roble, R. G. (1992). A thermosphere/ionosphere general circulation model with coupled electrodynamics. *Geophysical Research Letters*, *19*(6), 601–604. https://doi.org/10.1029/92GL00401

Shume, E. B., Denardini, C. M., de Paula, E. R., & Trivedi, N. B. (2010). Variabilities of the equatorial electrojet in Brazil and Perú. *Journal of Geophysical Research*, *115*, A06306. https://doi.org/10.1029/2009JA014984

Siddiqui, T. A., Stolle, C., Lühr, H., & Matzka, J. (2015). On the relationship between weakening of the northern polar vortex and the lunar tidal amplification in the equatorial electrojet. *Journal of Geophysical Research: Space Physics*, *120*, 10,006–10,019. https://doi.org/10.1002/2015JA021683

Singh, D., Gurubaran, S., & He, M. (2018). Evidence for the influence of DE3 tide on the occurrence of equatorial counterelectrojet. *Geophysical Research Letters*, *45*, 2145–2150. https://doi.org/10.1002/2018GL077076

Soares, G. B., Matzka, J., & Pinheiro, K. (2018). Preliminary minute means Geomagnetic Observatory Tatuoca (TTB), 2008 to 2017. V. 1. GFZ Data Services. http://doi.org/10.5880/GFZ.2.3.2018.005

Stening, R. J., Meek, C. E., & Manson, A. H. (1996). Upper atmosphere wind systems during reverse equatorial electrojet events. *Geophysical Research Letters*, *23*(22), 3243–3246. https://doi.org/10.1029/96GL02611

Stolle, C., Manoj, C., Lühr, H., Maus, S., & Alken, P. (2008). Estimating the daytime equatorial ionization anomaly strength from electric field proxies. *Journal of Geophysical Research*, *113*, A09310. https://doi.org/10.1029/2007JA012781

Sugiura, M., & Fanselau, G. (1966). Lunar phase numbers ν and ν′ for years 1850 to 2050. (Report X-612-66-401). Greenbelt, Mayland: Goddard Space Flight Center.

Thébault, E., Finlay, C. C., Beggan, C. D., Alken, P., Aubert, J., Barrois, O., et al. (2015). International geomagnetic reference field: The 12th generation. *Earth, Planets and Space*, *67*(1), 1–19. https://doi.org/10.1186/s40623-015-0228-9

Valladares, C. E., & Chau, J. L. (2012). The low-latitude ionosphere sensor network: Initial results. *Radio Science*, *47*, RSOL17. https://doi.org/10.1029/2011RS004978

Venkatesh, K., Fagundes, P. R., Prasad, D. S. V. V. D., Denardini, C. M., de Abreu, A. J., de Jesus, R., & Gende, M. (2015). Day-to-day variability of equatorial electrojet and its role on the day-to-day characteristics of the equatorial ionization anomaly over the Indian and Brazilian sectors. *Journal of Geophysical Research: Space Physics*, *120*, 9117–9131. https://doi.org/10.1002/2015JA021307

Vichare, G., & Rajaram, R. (2011). Global features of quiet time counterelectrojet observed by Ørsted. *Journal of Geophysical Research*, *116*, A04306. https://doi.org/10.1029/2009JA015244

Yamazaki, Y. (2013). Large lunar tidal effects in the equatorial electrojet during northern winter and its relation to stratospheric sudden warming events. *Journal of Geophysical Research: Space Physics*, *118*, 7268–7271. https://doi.org/10.1002/2013JA019215

Yamazaki, Y., & Kosch, M. J. (2015). The equatorial electrojet during geomagnetic storms and substorms. *Journal of Geophysical Research: Space Physics*, *120*, 2276–2287. https://doi.org/10.1002/2014JA020773

Yamazaki, Y., & Maute, A. (2017). Sq and EEJ—A review on the daily variation of the geomagnetic field caused by ionospheric dynamo currents. *Space Science Reviews*, *206*(1-4), 299–405. https://doi.org/10.1007/s11214-016-0282-z

Yamazaki, Y., & Richmond, A. D. (2013). A theory of ionospheric response to upward-propagating tides: Electrodynamic effects and tidal mixing effects. *Journal of Geophysical Research: Space Physics*, *118*, 5891–5905. https://doi.org/10.1002/jgra.50487

Yamazaki, Y., Yumoto, K., Yoshikawa, A., Watari, S., & Utada, H. (2009). Characteristics of counter-Sq SFE (SFE*) at the dip equator CPMN stations. *Journal of Geophysical Research*, *114*, A05306. https://doi.org/10.1029/2009JA014124

Yizengaw, E., Moldwin, M. B., Zesta, E., Biouele, C. M., Damtie, B., Mebrahtu, A., et al. (2014). The longitudinal variability of equatorial electrojet and vertical drift velocity in the African and American sectors. *Annales Geophysicae*, *32*(3), 231–238. https://doi.org/10.5194/angeo-32-231-2014

Zhang, R., Liu, L., Le, H., & Chen, Y. (2017). Equatorial ionospheric electrodynamics during solar flares. *Geophysical Research Letters*, *44*, 4558–4565. https://doi.org/10.1002/2017GL073238

Zhang, R., Liu, L., Le, H., Chen, Y., & Kuai, J. (2017). The storm time evolution of the ionospheric disturbance plasma drifts. *Journal of Geophysical Research: Space Physics*, *122*, 11,665–11,676. https://doi.org/10.1002/2017JA024637